Accounting for spatial variability in nonlinear dynamic analyses of embankment dams on liquefiable deposits

By

Nicholas A. Paull, A.M.ASCE
Corresponding Author: Ph.D. Candidate, Department of Civil and Environmental Engineering, University of California, Davis, CA 95616, napaull@ucdavis.edu

Ross W. Boulanger, Ph.D., P.E., F.ASCE
Professor, Department of Civil and Environmental Engineering, University of California, Davis, CA 95616, rwboulanger@ucdavis.edu

Jason T. DeJong, Ph.D., M.ASCE
Professor, Department of Civil and Environmental Engineering, University of California, Davis, CA 95616, jdejong@ucdavis.edu

JGGE 146(11), DOI: 10.1061/(ASCE)GT.1943-5606.0002372
Authors' final copy
2020

Abstract

Nonlinear dynamic analyses (NDAs) of embankment dams of different heights founded on a spatially variable, liquefiable alluvial layer are used to examine factors influencing embankment deformations and develop guidance on selecting representative properties for uniform analysis models. Simulations are presented for embankments ranging from 5 m to 45 m high on stochastic and uniform alluvial layers subjected to a range of input motions, with sensitivity cases including the effects of various parameters describing the alluvium and embankments. Crest settlements and slope displacements obtained from the analyses with stochastic and uniform alluvial layers are compared to obtain equivalent uniform or representative percentile properties for which a uniform model produces the same deformation as a stochastic model. The representative percentile properties to estimate median deformations from a set of stochastic realizations are generally between the 40^{th} and 60^{th} percentile, whereas the representative percentile properties to estimate deformations conservatively (i.e., exceeded in less than 16% of the analysis cases) are generally closer to the 30^{th} percentile. The variability in deformation patterns obtained with the stochastic models increases as the alluvium's scale of fluctuation in the horizontal direction increases relative to the embankment base width. Recommendations regarding factors to consider in selecting representative properties for spatially variable alluvial foundations in NDAs of embankment dams and the corresponding variability in deformations are presented.

Introduction

Spatial variability of liquefiable soil strata is an important consideration for seismic performance evaluations of geotechnical systems. Spatial variability in a stratum can be directly incorporated into a nonlinear dynamic analysis (NDA) model using probabilistic methods (hereafter called stochastic models), although this approach is not yet common in earthquake engineering practice. More commonly, spatial variability in a stratum is indirectly accounted for by selecting representative properties that are uniformly applied to the entire stratum (hereafter called uniform models). "Representative" properties are defined herein as those that, when used in a uniform model, produce deformations that are comparable to the deformations from a stochastic model.

A limited number of studies have examined factors that influence the selection of representative properties for liquefiable strata in an NDA, although additional influencing factors can be inferred from studies for other types of geotechnical problems. For example, representative properties for a stratum can generally be expected to depend on the scale of the structure or failure mechanism being analyzed, the scales of fluctuation in the stratum, and the mechanism of deformation (Baecher and Christian 2003). Regarding liquefaction of level sites, Popescu et al. (1997, 2005) performed two- and three-dimensional NDAs with stochastic and uniform soil properties and concluded that the pore pressure generation and triggering of liquefaction was best approximated using uniform models assigned the 20^{th} percentile values of the properties in the stochastic models. Perlea and Beaty (2010) summarized some common practices in NDAs of embankment dams using uniform models. They noted that cyclic resistance ratios (CRR) are often based on 33^{rd} percentile penetration resistances (e.g., Standard Penetration Test (SPT) or Cone Penetration Test (CPT) overburden and energy corrected, equivalent clean sand $(N_1)_{60cs}$ or q_{c1Ncs} values) and post-liquefaction residual shear strengths (S_r) are often based on 33^{rd} to 50^{th} percentile penetration resistances. These practices appear to be based on engineering judgments rather than formal comparisons of stochastic and uniform model responses. Montgomery and Boulanger (2016) performed 2D NDAs of infinite slopes and showed that the representative percentile (P_{rep}) to estimate the median value of lateral spreading displacement from stochastic models also generally ranged from the 30^{th} to 70^{th} percentile. The smaller P_{rep} values corresponded to thicker crust layers, thicker liquefiable layers, greater slope angles, and the lower range of the imposed shaking intensities; these conditions appeared to enable shear deformations to more easily develop through interconnected networks of looser lenses. Boulanger and Montgomery (2016) performed 2D NDAs of a 45 m high embankment on a 3 m or 12 m thick alluvial layer, and showed that the P_{rep} to estimate the median values of dam crest settlement or embankment shell deformation from stochastic models generally ranged from the 30^{th} to 70^{th} percentile. The smaller P_{rep} values corresponded to the thicker sand layer and the lower range of the imposed shaking intensities; these analyses used a horizontal scale of fluctuation (θ_x) of 20 m, which is a small fraction of the base width of the embankment. Paull et al. (2019) presented preliminary results for different size embankments on

liquefiable alluvium that show P_{rep} and deformation variability depends on the scales of fluctuation in soil properties relative to the dimensions of the embankment and foundation layer. These findings are consistent with findings from other researchers looking at geotechnical systems such as footings, retaining walls and slopes (e.g.; Baecher and Christian 2003, Fenton and Griffiths 2008, Joint TC205/TC304 Working Group 2017) but additional work was needed to quantify these dependencies and develop recommendations for NDAs of embankment dams founded on liquefiable soils.

The present study used nonlinear dynamic analyses (NDAs) of embankment dams of different heights founded on a spatially-variable, liquefiable foundation layer to examine factors influencing dam deformations and develop guidance on selecting representative properties for uniform models. The numerical simulations used the finite different program FLAC (Itasca 2016) with the user-defined constitutive model PM4Sand (Boulanger and Ziotopoulou 2017) for the liquefiable soils. Simulations are presented for "stochastic models" with spatially correlated Gaussian random fields of $(N_1)_{60cs}$ values for the liquefiable layer and "uniform models" with a single $(N_1)_{60cs}$ value for the liquefiable layer. Crest settlements and slope displacements are compared to obtain equivalent uniform or representative $(N_1)_{60cs}$ values (expressed as a representative percentile, P_{rep}, of the stochastic distributions) for which a uniform model produces the same deformation as a stochastic model. Simulations are performed for embankment dams of four different heights (H = 5, 10, 25, and 45 m) subjected to a range of input motions with different characteristics and intensities. Sensitivity analyses are used to examine the effects of horizontal and vertical scales of fluctuation for the liquefiable layer, mean value and coefficient of variation (COV) for the $(N_1)_{60cs}$ values in the liquefiable layer, thickness of the liquefiable layer, inclusion of a clay core trench through the liquefiable layer, constitutive model used to represent the clay core, and strengths assigned to the compacted embankment. Recommendations regarding factors to consider in selecting representative properties for spatially variable alluvial foundations in NDAs of embankment dams, and the corresponding variability in deformations that might reasonably be accounted for, are presented.

NDA Embankment Models

This section describes the embankment and foundation configurations, material properties and constitutive model calibrations, stochastic and uniform model parameters, initialization of static stress conditions, and dynamic loading procedures. The details of these modeling procedures and input parameters all have an influence on the deformations obtained in an NDA. Furthermore, the overall accuracy of any NDA modeling procedure is dependent on limitations inherent to continuum modeling, constitutive models, and numerical procedures. Despite these challenges, the representative percentile properties obtained by comparing the deformations from stochastic and uniform analysis models are less sensitive to variations in the modeling procedures and input parameters, provided that they are kept consistent between the two types of analyses.

Embankment and Foundation Configurations

Embankments with heights of 5, 10, 25 and 45 m, as shown in Figure 1, were modeled analyzed using the FLAC 8.0 finite difference program (Itasca 2016). Each embankment has a 6 m wide crest with upstream slopes at 2.5:1 (H:V) and downstream slopes that transition from 2.5:1 near the crest to 3.5:1 over the lower portions. The pre-shaking embankment heights (H) and base lengths (B) for the different size embankment models are listed in Table 1. Each embankment is founded on a 12 m thick alluvial layer, which is underlain by a 15 m thick bedrock layer. The embankments have upstream and downstream shells of cohesionless soils, and a central clay core that, for the highest embankment, extended through the alluvium to bedrock. The freeboard between the reservoir level and embankment crest is 25% of the embankment height. Variations in the alluvium thickness and central core geometry are examined as part of the sensitivity studies presented later.

Material Properties and Constitutive Model Calibrations

The bedrock is modeled as linear elastic with a Poisson's ratio of 0.3, a shear modulus of 1800 MPa, and a saturated density, ρ, of 2.2 Mg/m^3, which correspond to a shear wave velocity, V_s, of 900 m/s. The bedrock permeability is 5.0×10^{-6} cm/s.

The clay core is modeled as a Mohr-Coulomb material with undrained shear strengths for the dynamic loading phase computed based on the initial static consolidation stresses

using the procedures in Duncan and Wright (2005) as applied to NDA models by Montgomery et al. (2014). The undrained shear strength parameters for isotropic consolidation are d_R = 33 kPa and ψ_R = 14°, and the drained shear strength parameters are d_S (or c') = 0 and ψ_S (or ϕ') = 36°. The shear modulus is set proportional to the square root of the mean effective stress (p'), with G = 43 MPa at p' = 101.3 kPa. The permeability is 5.0×10^{-5} cm/s and the saturated density is 2.0 Mg/m^3. Sensitivity analyses examine use of the PM4Silt constitutive model (Boulanger and Ziotopoulou 2019) and reduced strength.

The shells are modeled using PM4Sand version 3.1 (Boulanger and Ziotopoulou 2017) with properties based on a uniform Standard Penetration Test (SPT) corrected blow count, $(N_1)_{60cs}$ = 35. The relative density (D_R) and shear modulus coefficient (G_o) are set based on the correlations presented in Boulanger and Ziotopoulou (2017). The contraction rate parameter (h_{po}) is calibrated based on single-element direct simple shear simulations to match the cyclic resistance ratio (CRR) based on the SPT based liquefaction triggering correlation from Boulanger and Idriss (2012). All remaining PM4Sand input parameters are set at the default values. The permeability is 5.0×10^{-4} cm/s and the saturated unit weight is 2.1 Mg/m^3. Sensitivity analyses examine the effect of a smaller $(N_1)_{60cs}$ = 21 for the shells.

The alluvial layer is also modeled using PM4Sand with the properties for each individual zone based on its assigned SPT $(N_1)_{60cs}$ value. SPT $(N_1)_{60cs}$ values are input as uniform values or as Gaussian random fields as described in the next section. The D_R, G_o and h_{po} are based on the same correlations and procedure described for the shells with all remaining PM4Sand input parameters set at their default values. The permeability is 5.0×10^{-4} cm/s and the total density is 2.0 Mg/m.

A Rayleigh damping of 0.5% at a frequency of 3 Hz was applied to all materials to provide a minimum level of damping in the small strain range for the nonlinear materials and a nominal damping for the elastic bedrock material.

Stochastic and Uniform Models for the Alluvial Layer

For the stochastic analyses, the alluvial layer is represented by a spatially correlated Gaussian random field (Vanmarke 2010) of $(N_1)_{60cs}$ values. Spatial variability in many depositional environments is often far more complex and scale-dependent than a Gaussian random field can accurately represent, but this idealization provides a means for

examining the effects of different parameters under a manageable range of conditions. The $(N_1)_{60cs}$ values then determine the input parameters for the constitutive model as described previously. The baseline realizations use a mean $(N_1)_{60cs}$ of 15 with a standard deviation in $(N_1)_{60cs}$ of 6 (i.e., coefficient of variation, COV, of 0.4), along with a horizontal scale of fluctuation (θ_x) of 20 m and a vertical scale of fluctuation (θ_y) of 1 m consistent with typical values reported in Phoon and Kulhawy (1999). The $(N_1)_{60cs}$ values were restricted to values of one or greater, which affected fewer than 0.5% of the alluvial elements in these realizations. The cumulative distributions of the $(N_1)_{60cs}$ values from seven realizations are plotted in Figure 2. Jaksa et al. (1997) observed that the statistics of soil deposits greatly depend on factors such as sample spacing, stationarity of the data, and measurement error. For this reason, the sensitivity studies presented later will examine a range of $(N_1)_{60cs}$ distributions and scales of fluctuation.

For the uniform analysis models, the alluvial layer was represented by $(N_1)_{60cs}$ values of 7.5, 10, 12.5, 15, 17.5, and 20, which are approximately the 10th, 20th, 33rd, 50th, 66th, and 80th percentiles of the $(N_1)_{60cs}$ distributions, respectively. The responses obtained with this range of uniform $(N_1)_{60cs}$ values were generally sufficient for estimating equivalent representative percentiles for the stochastic analyses.

Initial Static Stress Conditions

Static stress and steady seepage conditions were initialized by simulating placement of the embankment in multiple lifts, followed by raising the reservoir level in a sequence of stages. The embankment and alluvial materials were modeled as Mohr-Coulomb materials with confinement-dependent moduli for these initial static analyses. The resulting distributions of pore water pressure, vertical effective stress, coefficient of lateral earth pressure at rest (K_o), and initial static shear stress ratio (α) were smoothly varying with distributions that were reasonable. The embankment and alluvial materials were then updated with their respective material models prior to dynamic loading.

Dynamic Loading

The baseline set of analyses used the three input ground motions shown in Figure 3. These motions are from the NGA-West2 database (Ancheta et al. 2014) and represent a range of ground motion durations and frequency contents. The Mudurnu station fault normal (FN) motion from the 1999 Duzce earthquake (M=7.1) is scaled to peak ground

accelerations (PGAs) of 0.4 g, 0.6 g and 0.8 g. The TCU075 station east-west recording from the 1999 Chi-Chi earthquake (M=7.6) is scaled to PGAs of 0.2 g, 0.4 g and 0.6 g. The TAPS pump station number 10-047 recording from the 2002 Denali earthquake (M=7.9) is scaled to PGAs of 0.2 g, 0.4 g and 0.6 g.

All motions are applied as a shear stress time series to the compliant base of the embankment models (Mejia and Dawson 2006) with free field conditions applied at the lateral boundaries (Itasca 2016). Alluvial elements connected to the lateral boundaries were modeled as linear-elastic with a secant shear modulus equal to 70% of the small strain shear modulus computed for its assigned $(N_1)_{60cs}$ value and confining stress. Columns of linear elastic material at the free-field boundaries avoid problems with lateral instability at the boundaries when adjacent materials liquefy during dynamic loading.

Other aspects of the dynamic simulations are as follows. The baseline simulations used undrained conditions during dynamic loading, while the role of pore pressure diffusion during shaking was examined as part of the sensitivity analyses. The PM4Sand calibrations used herein result in undrained critical state shear strengths that are sufficient for the embankments to remain stable at end of dynamic loading, such that the embankment deformations are controlled by cyclic mobility behaviors. In practice, a case history based estimate of residual shear strength is often imposed at the end of strong shaking (e.g., Boulanger et al. 2015), but this step was not included herein, except for in a single set of sensitivity analysis cases, because the focus was on examining cyclic mobility aspects of dam deformation. Numerical solutions were checked for sensitivity to the mesh (coarser meshes gave similar responses within a few percent) and the numerical time step (smaller time steps had negligible effect on responses). Computation times on a multicore workstation ranged from 6 to 24 hours depending on the ground motion and other parameters.

Dynamic Analyses Results for Baseline Cases

The dynamic responses of the uniform and stochastic analysis models are compared in terms of the embankment displacements after the end of seismic loading. Other measures of dynamic response can be important in certain situations, but embankment displacements are generally a primary concern in seismic evaluations. Displacements compared in these analyses include crest settlement, embankment stretch and

embankment translation. Crest settlements are obtained as the vertical deformation of the embankment crest which is often used to assess the potential for loss of freeboard, cracking, or uncontrolled release of a reservoir. Embankment stretches are the increase in embankment base length (ΔB) taken as the difference in the horizontal displacements of the embankment toes. Embankment stretch is preferred over using the displacements of the two toes separately, because stochastic realizations sometimes result in a large outward displacement at one toe or the other, and the statistics on embankment stretch (which reflects large displacements at either toe) are better behaved than the statistics for displacement at either toe alone. Embankment translations are obtained as the average of the horizontal upstream and downstream toe displacements used to assess the overall horizontal movement of the embankment. The analysis cases presented herein involve crest settlements that range from 0.09 m to 2.9 m, (0.5% to 22% in terms of the percent of the embankment height); parameter sets that produce smaller or larger deformations are of less practical interest for developing guidance on selecting representative percentiles. The computational time required for each analysis imposed limits on the number of simulation cases that could be explored, and thus emphasis is given to those findings that are most strongly evident in the results and unlikely to be sensitive to the number of simulations performed.

Dependence of Representative Percentiles on Deformation Mechanisms

The determination of representative percentiles for the alluvial layer is illustrated using the deformation results, obtained at the end of shaking, shown in Figure 4 for the 10 m high embankment subjected to the TAPS motion scaled to an outcrop PGA of 0.6 g. The crest settlement was 1.0 m for the "uniform" analysis case with an $(N_1)_{60cs}$ of 15 for the alluvium (Figure 4a), and was 0.69 m for the uniform analysis case with an $(N_1)_{60cs}$ of 17.5 for the alluvium (Figure 4c). The crest settlement was 0.74 m for the analysis case using stochastic realization 1 for the alluvium (Figure 4b). It is estimated, using linear interpolation, that a uniform analysis model having an $(N_1)_{60cs}$ of 17.2 would have produced the same crest settlement as the stochastic model. These uniform $(N_1)_{60cs}$ values of 15, 17.2, and 17.5 correspond to the 50^{th}, 64^{th}, and 66^{th} percentile values for all the $(N_1)_{60cs}$ values in the stochastic realization, respectively (see Figure 2). Thus, for the stochastic analysis case shown in Figure 4c, the representative percentile of $(N_1)_{60cs}$ that

would produce the same crest settlement (P_{set}) in a uniform analysis model is P_{set} = 64%. In the event that a stochastic model produces a deformation that is less than obtained using the uniform model with the greatest assigned alluvial $(N_1)_{60cs}$ value (i.e., the 80th percentile value), the P_{rep} value is said to be > 80% and is set equal to 90% for calculating distributions of representative percentiles. In the event that a stochastic model produces a deformation that is greater than obtained using the uniform model with the smallest assigned alluvial $(N_1)_{60cs}$ value (i.e., the 10th percentile value), the P_{rep} value is said to be < 10% and is set equal to 5% for calculating distributions of representative percentiles.

Deformation patterns obtained for a stochastic model are generally more complex than for uniform analysis models, such that representative percentiles depend on the measure of deformation being considered. For example, the shear strain and deformation patterns for the stochastic model shown in Figure 4b are significantly more complex than for the uniform models shown in Figures 4a and 4c. The complexity of deformation patterns with stochastic models is further illustrated by the results shown in Figure 5 for the 10 m and 45 m high embankments with different stochastic realizations subjected to the Mudurnu motion scaled to an outcrop PGA of 0.8 g. The 10 m high embankment with stochastic realization 1 (Figure 5a) developed a crest settlement of 0.44 m, an embankment stretch of 0.7 m and an overall downstream translation of 1.85 m (i.e., the upstream and downstream toes translated 1.5 m and 2.2 m downstream, respectively). The corresponding representative percentiles for crest settlement, stretch, and translation were P_{set} > 80%, P_{str} > 80%, and P_{trans} = 35%. The deformations for the same embankment and motion with stochastic realization 2 (Figure 5b) included a greater crest settlement (0.79 m), greater stretch (1.24 m), and slightly smaller translation (1.19 m), with the representative percentiles showing similar changes to P_{set} = 23%, P_{str} = 18%, and P_{trans} = 73%. The 45 m high embankment with this same stochastic realization and motion (Figure 5c) as the embankment in Figure 5b had more than twice the crest settlement (1.9 m) and stretch (3.2 m) compared to the 10 m high embankment, but about half the translation (0.6 m). These examples illustrate that the: (1) deformation mechanisms are generally associated with greater shear strains in the looser zones of the alluvium, (2) extent and connectivity of looser zones beneath an embankment strongly affects the relative magnitudes of the outward displacements at either or both toes, the overall

translation of the embankment, and the crest settlement, and (3) values of P_{set}, P_{str}, and P_{trans} can be significantly different from each other for the same realization, particularly for the smaller embankments.

Representative Percentiles for Embankments with Different Heights

Representative percentiles for crest settlement and embankment stretch for the baseline set of stochastic models are plotted versus the normalized horizontal scale of fluctuation for the alluvial layer ($NSF_x = \theta_x/B$, where B is the width of the embankment base per Figure 1) in Figures 6a and 6b, respectively. These results are for the four embankments (H = 45, 25, 10, and 5 m) with seven realizations for the alluvium subjected to three input motions scaled to three different PGAs (a total of 63 cases for each size embankment dam). The θ_x is 20 m for these sets of realizations, such that θ_x/B increases with decreasing B and hence decreasing H. The median value for P_{set} and P_{str} at each θ_x/B (diamond symbols in Figures 6a and 6b) ranged from the 41st to 58th percentile with no clear dependence on θ_x/B. The sample standard deviations (calculated based on Johnson and Bhattacharyya 2010) and estimated standard deviations (calculated based on Lacasse and Nadim 1996) were used to compare the distributions of representative percentiles. A comparison of the two methods produced generally negligible differences and therefore, the sample standard deviations are provided herein. The sample standard deviations in P_{set} and P_{str} (denoted as σ_{Pset} and σ_{Pstr}) at each θ_x/B (Figures 6c and 6d) increased significantly with increasing θ_x/B. The σ_{Pset} and σ_{Pstr} were 3-5% for the largest embankment (H = 45 m, $\theta_x/B = 0.08$), 11-16% for the next largest embankment (H = 25 m, $\theta_x/B = 0.14$), and about 20% or more for the smaller embankments (H = 5 or 10 m, $\theta_x/B = 0.35$ or 0.76). The σ_{Pset} and σ_{Pstr} values are small for the H = 45 m embankment because its deformation mechanisms engage volumes of alluvial soil that are several times longer than the typical length of any looser lens, such that there is more averaging of shear resistances from both looser and denser zones. The σ_{Pset} and σ_{Pstr} are large for the H = 5 and 10 m embankments because their deformation mechanisms engage relatively small volumes of alluvial soil. For these smaller embankments, realizations with relatively large zones of looser soils beneath the embankment can experience significantly larger deformations (i.e., low P_{rep}) whereas realizations with relatively large zones of denser soils beneath the embankment can experience significantly smaller

deformations (i.e., high P_{rep} values). Similarly, the σ_{Pstr} are larger than the σ_{Pset} for each of the embankment heights (i.e., Figure 6c versus 6d) because horizontal displacements at either the upstream or the downstream toe are more sensitive to local variations than is the crest settlement.

Effect of ground motion

The effect of the ground motion on representative percentiles and their standard deviations is illustrated in Figure 7 for the same baseline results categorized by input motion. The median P_{set} (Figure 7a) and P_{str} (Figure 7b) for each of the scaled input motions were within a few percent of the overall median for the H =45 m embankment, whereas the variation relative to the overall median increased with decreasing embankment height (i.e., increasing θ_x/B). The σ_{Pset} and σ_{Pstr} values for each scaled input motion were generally smaller than for the full dataset, which illustrates that the ground motions are a significant contributor to variability in the P_{rep} values.

Sensitivity Analyses

Scales of Fluctuation in the Alluvium

The effect that the alluvial θ_x has on representative percentiles is illustrated in Figure 8, which shows P_{set} and P_{str} versus θ_x/B for the baseline cases (with θ_x = 20 m) in combination with additional results for θ_x = 10 m and 60 m with the H = 10 m and 25 m embankments and the full set of baseline motions. These additional cases correspond to θ_x/B values of 0.07, 0.18, 0.42, and 1.05, which span the full range of values generated in the baseline cases (i.e., using θ_x = 20 m with H = 5 to 45 m) and remain generally consistent with typical values reported in Phoon and Kulhawy (1999). The median P_{set} and P_{str} (Figures 8a and 8b) and the σ_{Pset} and σ_{Pstr} values (Figures 8c and 8d) obtained using θ_x = 10 m and 60 m follow the same general trends exhibited by the baseline cases. However, for the 25 m embankment case with θ_x = 60 m (θ_x/B = 0.42) the median P_{set} of about 32% was significantly less than for the other analysis cases. This is attributed to the occurrence of large shear strains in single weak layers that spanned from below the upstream to downstream shell in some realizations, therefore producing larger deformations and lower P_{set} values. These results suggest that the variability in P_{rep} values can be strongly dependent on θ_x/B, as expected.

The effect that the alluvial θ_y has on representative percentiles is illustrated in Figure 9, which shows P_{set} and P_{str} (Figures 9a and 9b) and σ_{Pset} and σ_{Pstr} values (Figures 9c and 9d) for four different combinations of θ_y and embankment height. The θ_y was doubled from 1.0 m (the baseline value) to 2.0 m for a set of analyses with the H = 25 m embankment, and halved from 1.0 m to 0.5 m for a set with the H = 10 m embankment. These values were chosen to remain generally consistent with typical values reported in Phoon and Kulhawy (1999). The full set of baseline input motions was used for all combinations. These variations in θ_y had relatively small effects on the median P_{rep} values or their standard deviations. These limited results are consistent with the expectation that variations in θ_x are likely to affect the embankment deformations more strongly than variations in θ_y for the range of conditions being examined herein and the deformation mechanism illustrated previously in Figures 4 and 5.

Property Distributions for the Alluvium

The effects of changing the alluvium's $(N_1)_{60cs}$ distribution are illustrated in Figure 10 which shows P_{set} and P_{str} (Figures 10a and 10b) and σ_{Pset} and σ_{Pstr} values (Figures 10c and 10d) for four different combinations of the mean and standard deviation in $(N_1)_{60cs}$ values. The H = 10 m and H = 25 m embankments are analyzed with sets of alluvial $(N_1)_{60cs}$ values generated for a mean of 15 with a COV of 0.2 or 0.4 and for a mean of 20 with a COV of 0.3 or 0.4. These values were chosen to remain consistent with typical values reported in Phoon and Kulhawy (1999). Note that the first category of data points plotted in Figure 10 are for the baseline case with a mean of 15 and COV of 0.4. The stochastic realizations for each analysis set were linearly transformed from the baseline stochastic realizations to maintain the same spatial distribution patterns while adjusting the mean and standard deviations. The TCU075 motion scaled to a PGA of 0.6 g was used for these analyses. The changes in the median P_{rep} values and their standard deviations were relatively small for this range of variations in the alluvium's $(N_1)_{60cs}$ distributions, and are not significant given the small number of realizations used for this comparison.

The effects of changing the alluvium's $(N_1)_{60cs}$ distribution from a normal distribution to a lognormal distribution was similarly examined using the H = 25 m embankment with a mean $(N_1)_{60cs}$ of 15 and COV of 0.4 subjected to the TCU075 motion scaled to a PGA

of 0.6 g. The stochastic realizations for the lognormal cases were transformed from the baseline stochastic realizations to maintain similar spatial distribution patterns. The median P_{rep} values and their standard deviations were relatively unaffected by the change in distribution form.

Alluvial Thickness

The effect of the alluvial layer thickness is illustrated in Figure 11 which shows P_{set} and P_{str} (Figures 11a and 11b) and σ_{Pset} and σ_{Pstr} values (Figures 11c and 11d) versus alluvial layer thickness for the H = 10 m embankment. Analysis models were developed with alluvial layer thicknesses of 3, 12, or 20 m. Twenty stochastic realizations were generated for each analysis model using the same baseline statistics and scales of fluctuation. The TCU075 motion scaled to a PGA of 0.6 g was used for these analyses. The median P_{set} and P_{str} do not change significantly with alluvial layer thickness, although the median P_{str} for a 20 m thick layer was 10% below that for the 12 m thick layer. The σ_{Pset} and σ_{Pstr} values were greatest for the 3 m thick layer, which is attributed to the smaller range in deformations from the uniform models.

Core Trench Geometry

The effect of having a core trench for the H = 45 m embankment (Figure 12a) was examined by repeating analyses with the core trench removed (Figure 12c). The same stochastic realizations were used for the two analysis models, with the core only replacing elements after the realization was generated. These analyses used the full set of baseline input motions and PGAs. In general, removal of the core trench allowed deformation mechanisms to coalesce along weaker zones that extended underneath the central portion of the dam foundation (Figures 12b versus 12d), thereby causing slightly greater crest settlements and outward toe displacements. The median P_{set} and P_{str} values did not change significantly because removing the core trench had similar effects on the uniform analysis models. The σ_{Pset} and σ_{Pstr} values, however, did increase significantly with the core trench removed; e.g., σ_{Pset} increased from 1% to 4%, σ_{Pstr} increased from 3% to 7%, and σ_{Ptrans} increased from 2% to 16%. These σ_{Prep} values are still less than for the H = 25 m embankment which also does not have a core trench (Figure 6), indicating that the differences in results for the H = 25 m and 45 m embankments are mostly attributable to their different θ_x/B values.

Embankment Strength

The effect of embankment soil strength was examined by repeating analyses for the H = 10 m and 45 m embankments with a reduced soil strength in the embankment shells and core. The $(N_1)_{60cs}$ in the shells are reduced 40%, from 35 to 21, and the undrained shear strengths for the clay core are reduced by 20%. The shear wave velocity for both the core and the shells are reduced by 10%. The TCU075 motion scaled to a PGA of 0.6 g was used for these analyses. The median P_{set} and P_{str} values did not change significantly because reducing the embankment strength increased deformations for both the stochastic and uniform analysis models. The σ_{Pset}, σ_{Pstr} and σ_{Ptrans} values, however, did increase significantly with a weaker embankment; e.g., for the H = 45 m embankment, σ_{Pset} increased from 2% to 6%, σ_{Pstr} increased from 3% to 13% and σ_{Ptrans} increased from 1% to 15%. The weaker embankment means that a greater proportion of the overall resistance to deformation comes from the alluvial layer. The result is that deformations are more sensitive to stochastic variations in the alluvium realizations and hence σ_{Pset}, σ_{Pstr} and σ_{Ptrans} increase.

Constitutive Model for the Clay Core

A set of analyses for the H= 10 m embankment were performed using the bounding surface plasticity PM4Silt model (Boulanger and Ziotopoulou 2019) for the clay core instead of the elastic-plastic Mohr-Coulomb model used in the baseline analyses. Input parameters for PM4Silt included the same shear strengths and densities as for the baseline analyses, along with $n^{b,wet} = 1.0$, $h_{po} = 400$, and $G_o = 870$. All other parameters retained their default values. The TCU075 motion scaled to a PGA of 0.6 g was used for these analyses. The median P_{set} and P_{str} and their standard deviations did not change significantly when the PM4Silt model was used in place of the Mohr-Coulomb model for the clay core.

Post-Shaking Residual Strengths

The 10 m high embankment models subjected to the TCU motion scaled to a PGA of 0.6g were used to assess how the selection of representative percentiles might be affected by reducing the undrained critical state shear strength to a case-history based residual strength at the end of strong shaking. Elements in both uniform and stochastic models (with θ_x= 20 m) were assigned a case-history based residual strength at the end of

shaking if their maximum shear strains exceeded 3% or their excess pore pressure ratios (r_u) exceeded 70% at any time during shaking. Residual strengths were calculated based on the strength ratio approach with potential void redistribution effects in Idriss and Boulanger (2015). The post-shaking analysis continued in time until the system reached a new static equilibrium. The embankment displacements increased by modest amounts for larger uniform blow counts, but more than doubled for smaller uniform blow counts. The median P_{set} decreased by 2 percentiles and P_{str} decreased by 15 percentiles, but the median P_{set} and P_{str} values remained greater than the 55th percentile and their standard deviations did not change significantly. Correlations for residual strength of liquefied soil have large uncertainty and therefore the choice of residual shear strength correlation can significantly affect post-shaking deformations. Further analyses evaluating the selection of representative properties for cases involving post-shaking instability are warranted.

Selection of Representative Percentiles for Uniform Analysis Models

The selection of representative percentiles for representing an alluvial layer in uniform analysis models depends on the analysis objectives. A representative percentile may be chosen to provide an unbiased estimate of the expected deformations, or a conservative estimate of the deformations, that would be obtained from stochastic analyses. For example, the cumulative distributions of the P_{set} and P_{str} values obtained from the baseline analyses for the four different size embankments are presented in Figures 13a and 13b, respectively. The slopes of these cumulative distributions progressively decrease with decreasing embankment height, which is another way of representing the increased variability in P_{set} and P_{str} values with decreasing embankment height. For an unbiased estimate of crest settlements (Figure 13a), it may be reasonable to use the overall median values for P_{set} which corresponds to $41\% \leq P_{set} \leq 58\%$ for the four embankment sizes. For an estimate of crest settlements that would only be exceeded in 16% of the cases, it may be reasonable to use the 16th percentile value for P_{set} which corresponds to $31\% \leq P_{set} \leq 34\%$ for the H = 5, 10 and 25 m embankments and P_{set} = 50% for the H = 45 m embankment. The representative percentiles to estimate embankment stretch or toe deformations are similar to slightly smaller than those to estimate crest settlement for the H = 10, 25, and 45 m embankments (Figure 13b). For the H = 5 m embankment, however, it would be necessary to use P_{str} = 33% for an unbiased

estimate of displacements and $P_{str} \approx 10\%$ for a reasonably conservative estimate of displacements. These results reflect the previous observation that, for the embankment models analyzed, the smallest embankment (largest θ_x/B) is most sensitive to the spatial variability of the alluvium, with local deformation mechanism (e.g., toe slumps) being especially sensitive.

The variability in deformations that is due to spatial variability in the alluvial layer is dependent on the same factors that affect the selection of P_{rep} for uniform analysis models. This component of deformation variability may be estimated using stochastic realizations or by repeating uniform analyses with an appropriate range of P_{rep} values (e.g., Figure 14). Deformation variability for the baseline cases examined herein is illustrated in Figure 14 showing the normalized crest settlement and embankment stretch from uniform analyses using the 50th percentile $(N_1)_{60cs}$ (Figures 14a and 14b), the 33rd percentile $(N_1)_{60cs}$ (Figures 14c and 14d), and the 20th percentile $(N_1)_{60cs}$ (Figures 14e and 14f) versus the values obtained from the stochastic analyses for all the input motions. Deformations for the H = 45 m embankment (blue "x" symbols) show the least variability in deformations, with the deformations computed using uniform analysis models with the 50th percentile $(N_1)_{60cs}$ being approximately equal to those from the stochastic analyses (i.e., the points are close to the 1:1 line in Figures 14a and 14b). Deformations for the other embankment heights are also approximately centered along the 1:1 line in Figures 14a and 14b, but the variability in deformations increases with as the embankment height decreases and is greater for embankment stretch than for crest settlement. The use of 33rd percentile $(N_1)_{60cs}$ in the uniform analysis models produces more conservative estimates of crest settlement and embankment stretch (Figures 14c and 14d), which shifts the points upward but does not significantly change their variability. For crest settlements, using 33rd percentile $(N_1)_{60cs}$ means that none of the data points for the H = 45 m embankment fall below the 1:1 line while 15-20% of the data points for the H = 5, 10 and 25 m embankments fall below the 1:1 line. For embankment stretch, using 33rd percentile $(N_1)_{60cs}$ is similarly conservative for the H = 10, 25, and 45 m embankments but 42% of the data points for the H = 5 m embankment are still below the 1:1 line. The use of 20th percentile $(N_1)_{60cs}$ adds additional conservatism for all embankments, but still leaves about 25% of the data points for the H = 5 m embankment below the 1:1 line (Figure

14f). These results are consistent with expectations based on Figure 13 as discussed previously.

The role of θ_x/B in selecting representative percentiles, as opposed to just embankment size, is illustrated in Figure 15 which shows cumulative distributions for P_{rep} for different combinations of H = 5, 10, and 25 m with θ_x = 10, 20, and 60 m. For an estimate of crest settlements that would only be exceeded in 16% of the cases, it may be reasonable to use P_{set} = 30% for most of these conditions. For an estimate of embankment stretch with this same level of conservatism, a lower P_{rep} becomes necessary once θ_x/B exceeds about 0.4 (i.e., cases with H = 10 m or 25 m and θ_x = 60 m). For such cases, it may be more appropriate to explicitly incorporate any identified, laterally extensive, weak layers into the uniform model to evaluate whether these extensive layers may dominate the shear strain behavior and cause additional deformations (as was the case with H = 25 m and θ_x = 60 m). These results illustrate that it is the larger θ_x/B conditions (i.e., smaller embankment size relative to θ_x) that can require consideration of the loosest conditions (e.g., P_{rep} as low as 5-10%) for estimating local deformations.

The role of deformations in the selection of representative percentiles is illustrated in Figure 16 which shows the representative percentiles obtained from normalized crest settlements and normalized stretches of the stochastic models for different combinations of H = 5, 10, 25, and 45 m with θ_x = 10, 20, and 60 m. For normalized crest settlements less than 1.5% (Figure 16a), the representative percentiles range from about 20% to 55% and were generally lower than those for larger deformations. The models that produce these smaller deformations develop r_u > 95% in less than 50% of the alluvium. In these cases, the lower representative percentiles are reflective of liquefaction only being triggered in the weaker portions of the alluvium. For the larger deformations, liquefaction occurs in most of the alluvium and the representative percentiles tend to larger on average. In these cases, the larger representative percentiles are attributed to the larger deformations engaging both stronger and weaker portions of the alluvium. Similar trends are illustrated for the embankment stretches (Figure 16b) where embankment stretches less than 0.4% generally produce representative percentiles less than 55%. However, since embankment stretches may be more affected by localized deformations near the embankment toes, some cases, especially with large θ_x/B, still produce larger

representative percentiles due to the presence of strong locations just beneath the embankment toes. These trends suggest that a lower representative percentile may be appropriate when liquefaction-induced deformations are relatively small and likely controlled by liquefaction triggering in only the looser portions of the deposit.

Discussion

The general observation that the distribution of P_{rep} values for an individual stratum and the deformation patterns for the overall system depend on the scale of fluctuation relative to the scale of the embankment (e.g., θ_x/B) is consistent with expectations based on prior studies for other types of geotechnical systems including footings, retaining walls and slopes (e.g., Baecher and Christian 2003, Fenton and Griffiths 2008, Joint TC205/TC304 Working Group 2017). The selection of representative percentiles has also been shown to depend on the amount of liquefied material in the foundation stratum and the scale of expected normalized deformations. In addition, it is likely that the distribution of P_{rep} will be affected to various degrees by factors not examined herein (e.g., constitutive model for the sands; hydraulic conductivities; reservoir level; stochastic modeling framework; three-dimensional effects), in addition to those factors examined in the sensitivity studies (e.g., ground motion characteristics, embankment strengths, system geometries). Precisely quantifying these secondary dependencies and their cross-correlations would take many times more simulations than were possible in the current study given the computational and manual interpretation demands. Nonetheless, the trends in the results presented herein are sufficient to demonstrate that the use and interpretation of uniform analysis models for assessing liquefaction effects would benefit from explicit consideration of the relative scales of an embankment and its deformation mechanisms to the scales of fluctuation in the liquefiable strata.

The use of conditioned stochastic realizations and site-specific ground motions in the seismic evaluation of an embankment on liquefiable soil could improve confidence in estimated embankment deformations in certain situations, and potentially provide value relative to the use of uniform analysis models. The variability in deformations obtained with conditioned stochastic realizations would be expected to decrease with increasing amounts or density of site exploration data, with the incremental benefits of additional explorations depending on the spacing of exploration borings/soundings relative to the

scales of fluctuation and embankment size. The engineering effort required to perform stochastic modeling is likely to reduce over time, such that the use of stochastic models may become preferable to the use of uniform analysis models when an explicit accounting of uncertainty is desired or the ultimate decision regarding potential modifications or actions is not clear.

Characterizing spatial variability in alluvial strata or other types of deposits requires a detailed geologic model and understanding of site-specific depositional processes, regardless of whether a stochastic or uniform analysis model is used. The geologic model provides a basis for identifying different strata that may have significantly different stochastic properties (e.g., property distributions or scales of fluctuation), and thus avoids the potentially obscuring effect of representing distinctly different strata together. The geologic model also provides a basis for refining site investigation studies, evaluating the potential for certain types of geologic features to have been missed by the site explorations, and constraining estimates for scales of fluctuation beyond what may be estimated using site exploration data alone. Stochastic realizations, conditioned on the available site exploration data, can be valuable for evaluating how the uncertainty in properties between exploration locations may affect performance, but their value is contingent on the geologic model being reasonably accurate.

Conclusions

Nonlinear dynamic analyses of different-height embankment dams (H = 5, 10, 25, and 45 m) on spatially-variable, liquefiable foundation layers were performed to examine factors that influence dam deformations and develop guidance to select representative properties for uniform models. Analyses were performed for stochastic models with spatially correlated Gaussian random fields of $(N_1)_{60cs}$ values for the liquefiable layer and uniform models with a single $(N_1)_{60cs}$ value for the liquefiable layer. These analyses correspond primarily to cases where the undrained critical state shear strengths are sufficient to maintain stability, and thus the results correspond to cases where deformations are largely controlled by cyclic mobility behaviors. Crest settlements and slope displacements were compared to obtain representative $(N_1)_{60cs}$ values (expressed as a representative percentile P_{rep} of the stochastic distributions) for which a uniform model produces comparable deformations as a stochastic model.

Embankment deformation patterns for stochastic models became increasingly variable between realizations as the normalized horizontal scale of fluctuation (θ_x/B) for the alluvium increased. The deformation variability was relatively small for cases with the smallest θ_x/B (e.g., θ_x/B = 0.08-0.14 for H = 25-45 m and θ_x = 20 m) because there was more averaging of shear resistances across looser and denser zones. Deformation variability became larger as θ_x/B increased because deformations became increasingly dependent on the location and connectivity of the looser zones in the foundation; e.g., the dominant deformation mechanisms with θ_x/B = 0.34-1.02 (for H =5-10 m and θ_x = 20-60 m) ranged from an overall downstream translation of the embankment to predominantly upstream and/or downstream slope movements. Uniform analysis models cannot reproduce the complexity or variability in potential deformation mechanisms for cases with relatively large θ_x/B, and this limitation must be recognized when uniform models are used to assess the consequences of liquefaction-induced deformations in relatively small embankments.

The selection of P_{rep} values to represent a liquefiable foundation layer in a uniform analysis model depends on the desired degree of conservatism, and the interpretation of the analysis results needs to consider the alluvium's horizontal scale of fluctuation relative to the scale of the embankment (e.g., θ_x/B). For an estimate of median crest settlement or median embankment slope displacements, it appears reasonable to use P_{rep} ≈ 45-50% for most situations. For a reasonably conservative estimate of crest settlement or embankment slope displacement (e.g., exceeded in less than 16% of the cases), it appears reasonable to use P_{rep} ≈ 30% for most cases, while recognizing the achieved level of conservatism may be less for cases involving localized deformations (e.g., at embankment toes with θ_x/B greater than about 0.4) or in cases with relatively small deformations associated with liquefaction triggering limited to only the loosest portions of a deposit. Localized deformations can be important for long, low-height embankment such as levees that could develop localized deformations over the loosest zones in an alluvial layer even if those loosest zones are relatively small in extent. In addition, the evaluation of liquefaction effects using uniform analysis models should consider uncertainty in P_{rep} values in combination with other uncertainties in the in-situ test and site characterization data as part of the expected sensitivity studies.

An accurate geologic model and understanding of site-specific depositional processes is essential for assessing liquefaction effects on embankments, regardless of whether stochastic or uniform analysis models are used. The geologic model provides a basis to identify distinctly different strata, refine site investigation studies, evaluate the potential for the site investigations to have missed important geologic features, and constrain estimates for scales of fluctuation beyond what may be estimated using site exploration data alone.

Data Availability Statement

Data that support the findings of this study available from the corresponding author upon reasonable request.

Acknowledgements

The work described herein progressed under projects for the California Department of Water Resources under Contract 4600009751 and the National Science Foundation under grant CMMI-1635398. Any opinions, findings, conclusions, or recommendations expressed herein are those of the authors and do not necessarily represent the views of these organizations. Professor Jack Montgomery provided assistance with the initial stochastic modeling. The anonymous reviewers provided valuable comments that improved the manuscript. The authors appreciate the above support and assistance.

References

Ancheta, T. D., Darragh, R. B., Stewart, J. P., Seyhan, E., Silva, W. J., Chiou, B. S. J., et al. (2014). NGA-West2 database. Earthquake Spectra EERI 2014; 30(3):989-1005.

Boulanger, R. W., and Idriss, I. M. (2012). "Probabilistic SPT-based liquefaction triggering procedure." Journal of Geotechnical and Geoenvironmental Engineering, ASCE, 138(10), 1185-1195.

Boulanger, R. W., Montgomery, J., and Ziotopoulou, K. (2015). "Nonlinear deformation analyses of liquefaction effects on embankment dams." Perspectives on Earthquake Geotechnical Engineering, A. Ansal and M. Sakr, eds., Geotechnical, Geological and Earthquake Engineering 37, 247-283, Springer, DOI 10.1007/978-3-319-10786-8_10

Boulanger, R. W., and Montgomery, J. (2016). "Nonlinear deformation analyses of an embankment dam on a spatially variable liquefiable deposit." Soil Dynamics and Earthquake Engineering, 91, 222–233.

Boulanger, R. W., and Ziotopoulou, K. (2019). "A constitutive model for clays and plastic silts in plane-strain earthquake engineering applications." Soil Dynamics and Earthquake Engineering, 127(2019): 105832, 10.1016/j.soildyn.2019.105832.

Boulanger, R. W., and Ziotopoulou, K. (2017). "PM4Sand (Version 3.1): A sand plasticity model for earthquake engineering applications", rep. No. UCD/CGM-17/01, Center for Geotechnical Modeling, Dept. of Civil and Environmental Engineering, Univ. of California, Davis, CA.

Baecher, G. B., and Christian, J. T. (2003). Reliability and statistics in geotechnical engineering. Wiley, Chichester, U.K., 619.

Duncan, J. M., and Wright, S. G. (2005). Soil strength and slope stability. J. Wiley & Sons, Hoboken.

Fenton, G. A., and Griffiths, D. V. (2008). Risk Assessment in Geotechnical Engineering. John Wiley & Sons, Inc., New York.

Idriss, I, M., and Boulanger, R. W. (2015). "2nd Ishihara Lecture: SPT- and CPT-based relationships for the residual shear strength of liquefied soils." Soil Dynamics and Earthquake Engineering, ASCE, 2015, 68, 57-68.

Itasca (2016). Fast Lagrangian Analysis of Continua (FLAC), release 8.0. Itasca Consulting Group, Inc., Minneapolis, MN.

Jaska, M. B., Booker, P. I., and Kaggwa, W. S. (1997). "Inaccuracies Associated with Estimation of Random Measurement Errors." Journal of Geotechnical and Geoenvironmental Engineering, ASCE, 1997, 123(5), 393-401.

Johnson, R. A., and Bhattacharyya, G. K. (2010). Statistics Principles and Methods. J. Wiley & Sons, Hoboken.

Joint TC205/TC304 Working Group (2017). "Discussion of statistical/reliability methods for Eurocodes – Final Report." 5th International Symposium on Geotechnical Safety and Risk, International Society for Soil Mechanics and Geotechnical Engineering, Rotterdam, Netherlands, 2015.

Lacasse, S., and Nadim, F. (1996). "Uncertainties in Characterizing Soil Properties". Uncertainty in the Geologic Environment from Theory to Practice Conference, Madison, WI, 1996.

Mejia, K. H., and Dawson, E. M. (2006). “4th International Symposium on Numerical Modeling in Geomechanics.” Minneapolis, MN.

Montgomery, J., Boulanger, R. W., Armstrong, R. J., and Malvick, E. J. (2014). “Anisotropic Undrained Shear Strength Parameters for Nonlinear Deformation Analyses of Embankment Dams.” Geo-Congress 2014 Technical Papers.

Montgomery, J., and Boulanger, R. W. (2016). "Effects of spatial variability on liquefaction-induced settlement and lateral spreading." Journal of Geotechnical and Geoenvironmental Engineering, ASCE, 2017, 143(1), 04016086, 10.1061/(ASCE)GT.1943-5606.0001584.

Paull, N. A., Boulanger, R. W., and DeJong, J. T. (2019). “Seismic deformations of different size embankments on a spatially variable liquefiable deposit.” Proc., 39th USSD Annual Meeting and Conference, United States Society on Dams, Chicago, IL, 2019.

Perlea, V. G., and Beaty, M. H. (2010) “Corps of Engineers practice in the evaluation of seismic deformation of embankment dams.” In Proceedings of the fifth international conference on recent advances in geotechnical earthquake engineering and soil dynamics. San Diego, CA.

Phoon, K.-K., and Kulhawy, F. H. (1999). “Characterization of geotechnical variability.” Canadian Geotechnical Journal, 36(4), 612–624.

Popescu, R., Prevost, J. H., and Deodatis, G. (1997). “Effects of spatial variability on soil liquefaction: some design recommendations.” Géotechnique, 47(5), 1019–1036.

Popescu, R., Prevost, J. H., and Deodatis, G. (2005). “3D effects in seismic lieuqfaction of stochastically variable soil deposits.” Géotechnique, 55(1), 21–31.

Vanmarcke, E. (2010). Random fields: analysis and synthesis. World Scientific, Hackensack, NJ.

Table 1: Embankment model dimensions.

Embankment Height, H (m)	Embankment Base Length, B (m)
45	249
25	138
10	57
5	26

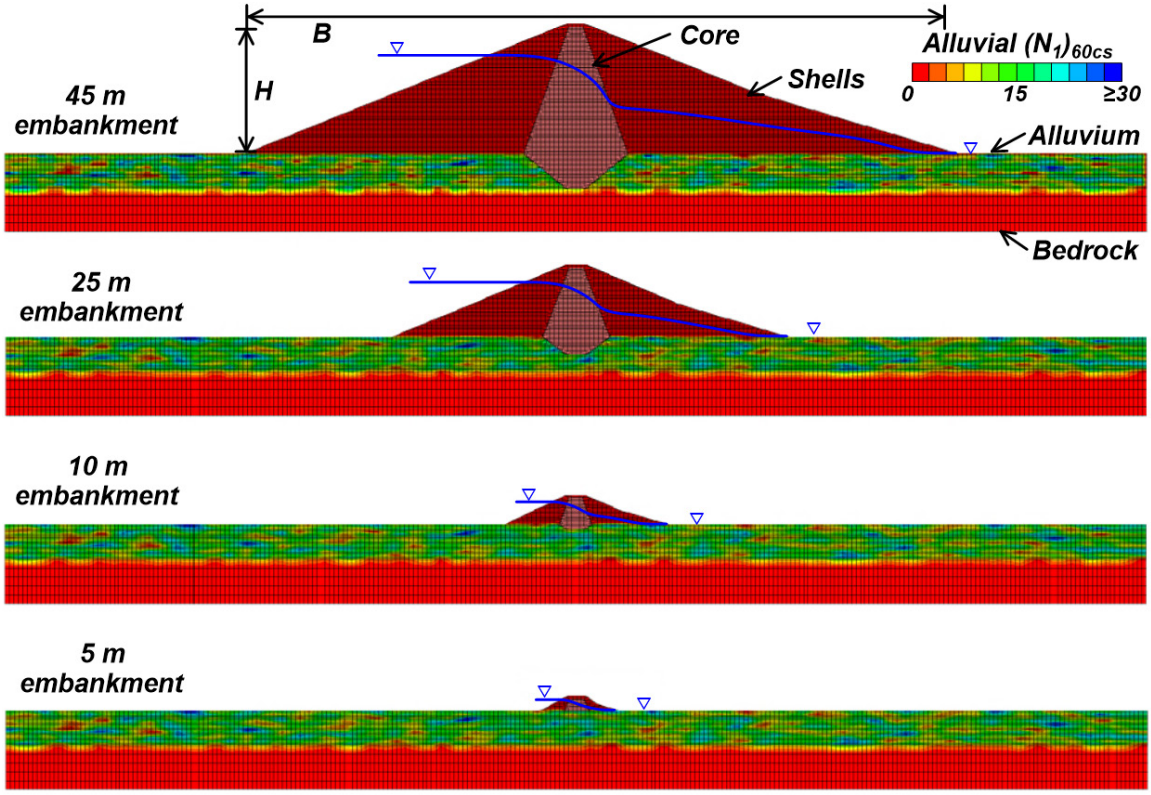

Figure 1: Embankment model geometries with the same realization of $(N_1)_{60cs}$ in the alluvium.

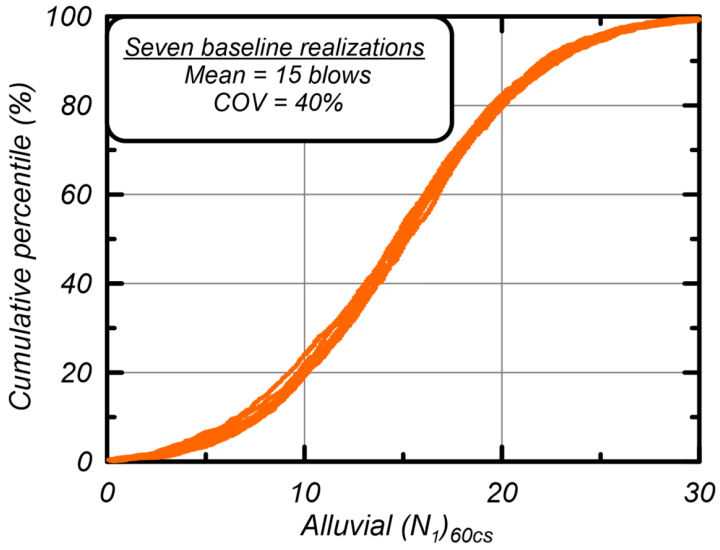

Figure 2: Cumulative distributions of $(N_1)_{60cs}$ from seven realizations for the alluvial layer.

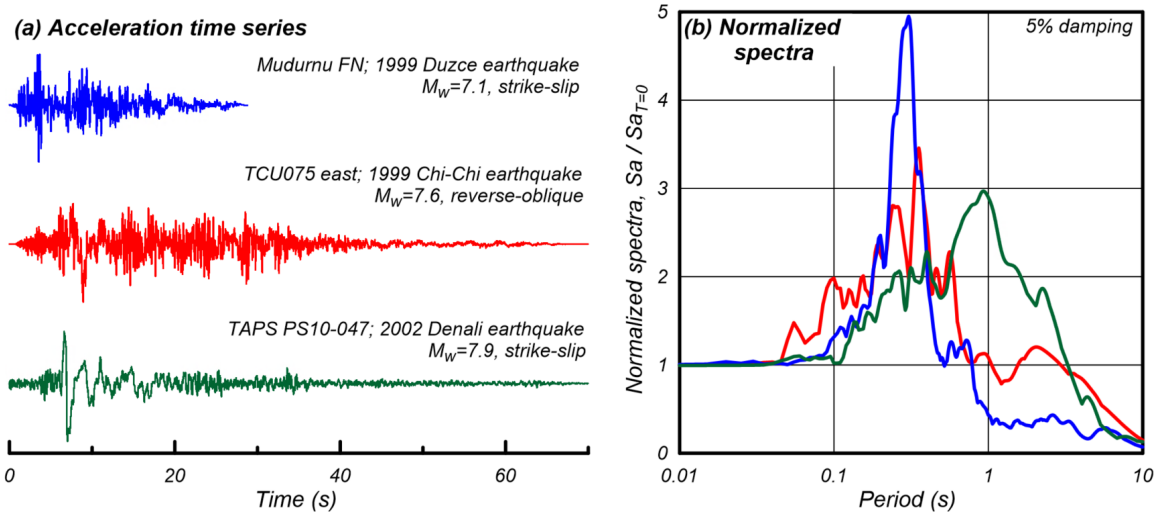

Figure 3: (a) Acceleration time series and (b) normalized spectra for input motions used in the baseline analyses (After Boulanger and Montgomery 2016).

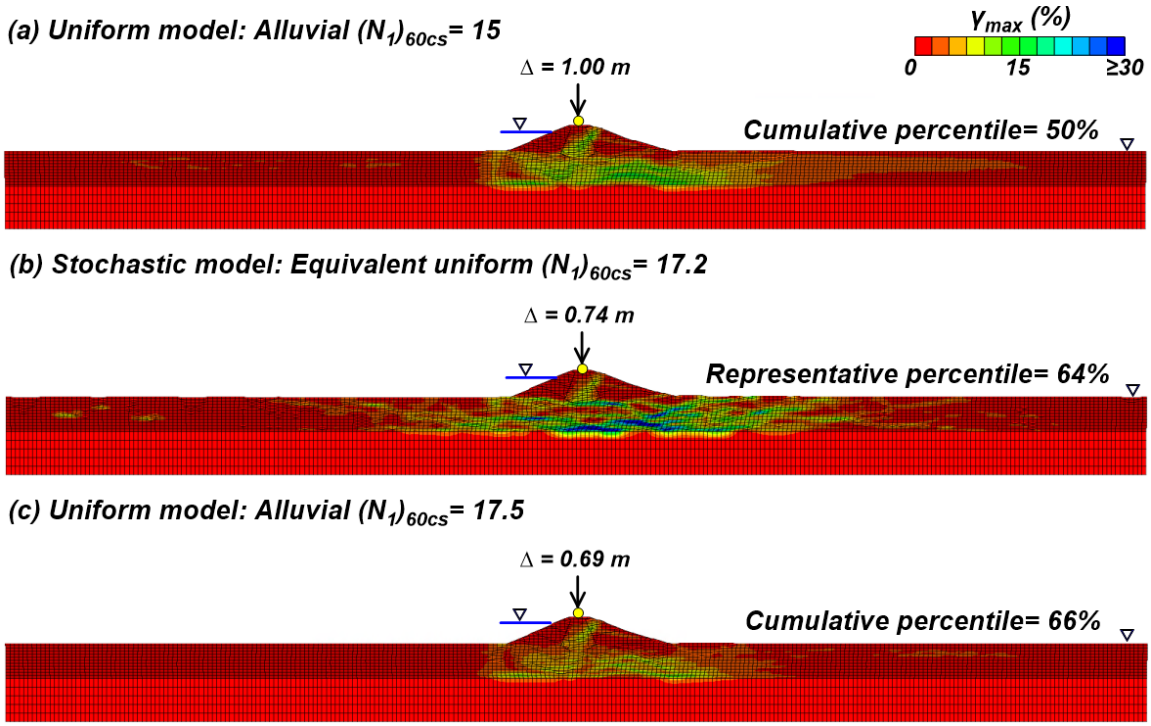

Figure 4: Deformation patterns and crest settlements for the 10 m high embankment models subjected to the TAPS motion scaled to a PGA of 0.6 g: (a) uniform model with alluvial $(N_1)_{60cs}$= 15, (b) stochastic model with realization 7 for the alluvium, and (c) uniform model with alluvial $(N_1)_{60cs}$ = 17.5.

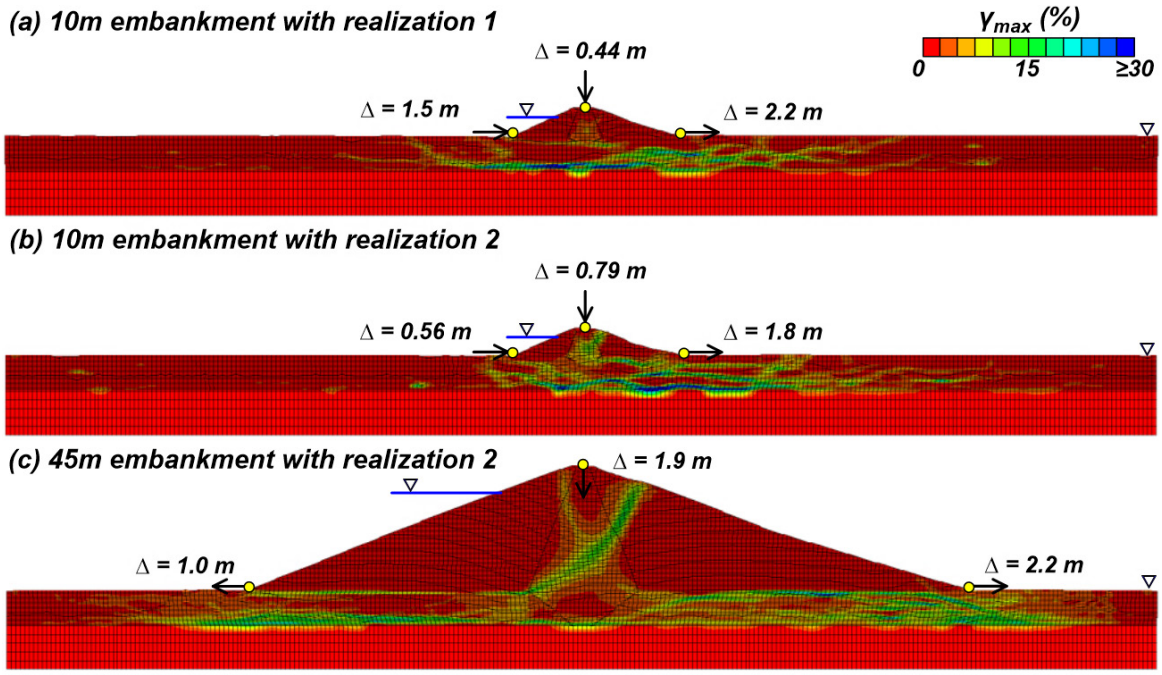

Figure 5: Maximum shear strains for stochastic models subjected to the Mudurnu motion scaled to 0.8 g with P_{rep} values: (a) $P_{set} > 80\%$, $P_{str} > 80\%$ and $P_{trans} = 35\%$, (b) $P_{set} = 23\%$, $P_{str} = 18\%$ and $P_{trans} = 73\%$ and (c) $P_{set} = 52\%$, $P_{str} = 60\%$ and $P_{trans} = 61\%$.

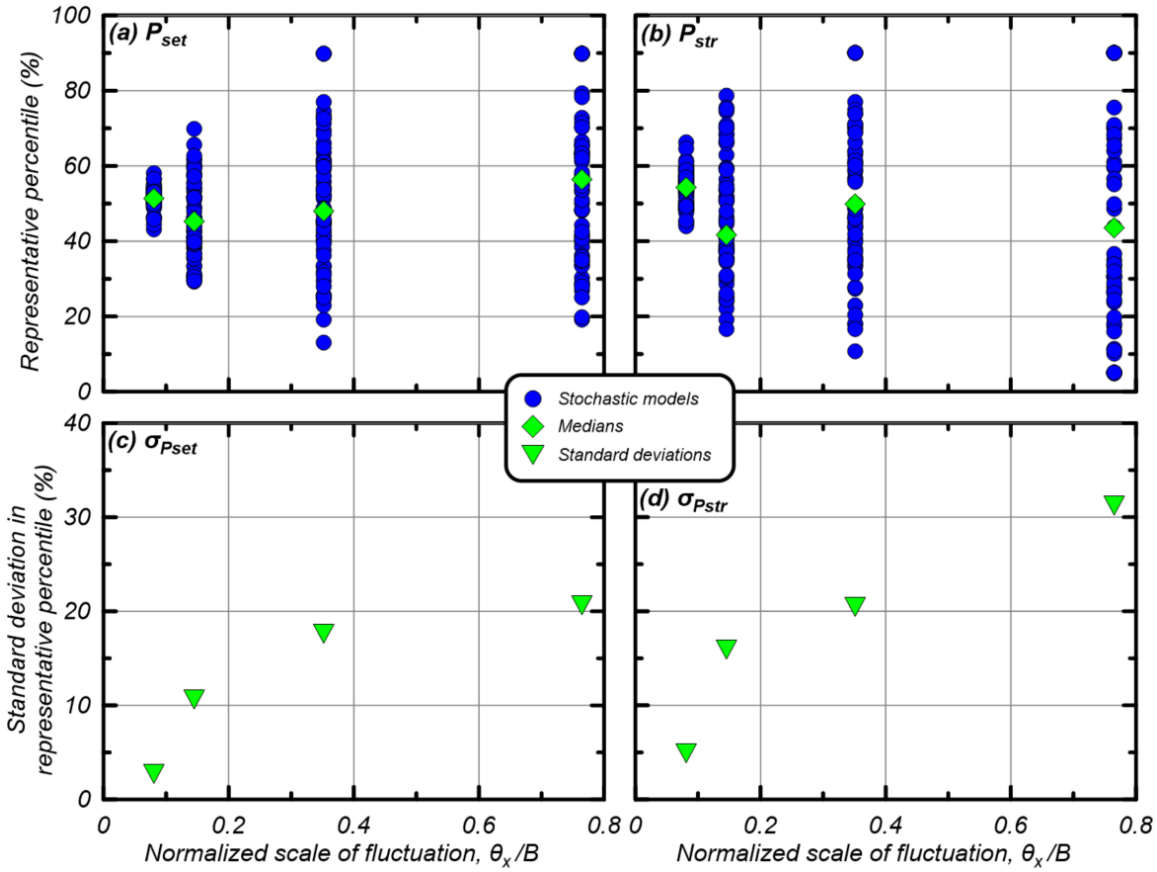

Figure 6: (a) P_{set}, (b) P_{str}, (c) σ_{Pset} and (d) σ_{Pstr} versus normalized scale of fluctuation (NSF_x) for the 5 m, 10 m, 25 m, and 45 m tall embankments with the baseline stochastic realizations for the alluvium (θ_x = 20 m), subjected to three motions scaled to three PGAs.

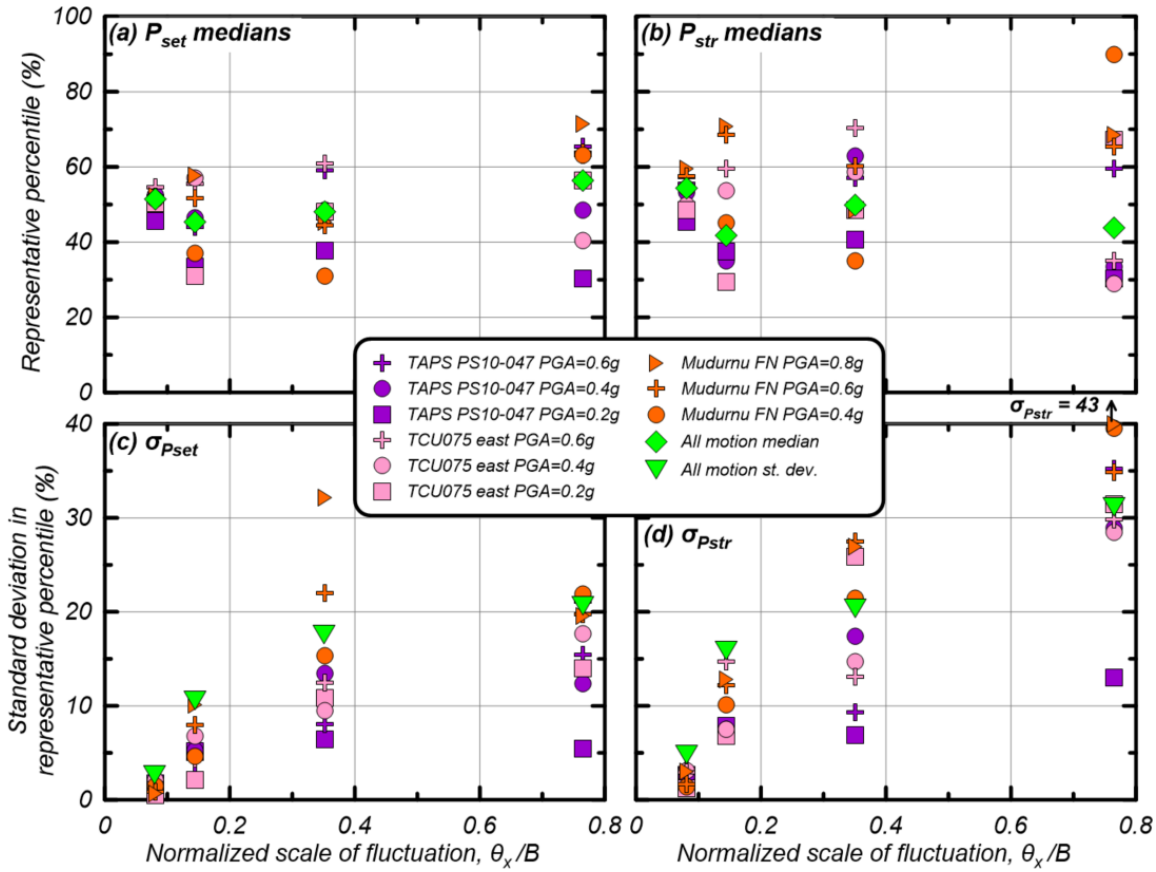

Figure 7: (a) P_{set} medians, (b) P_{str} medians, (c) σ_{Pset} and (d) σ_{Pstr} versus NSF_x for the 5 m, 10 m, 25 m, and 45 m tall embankment dam cases with the baseline stochastic realizations (θ_x = 20 m) deaggregated by PGA and motion.

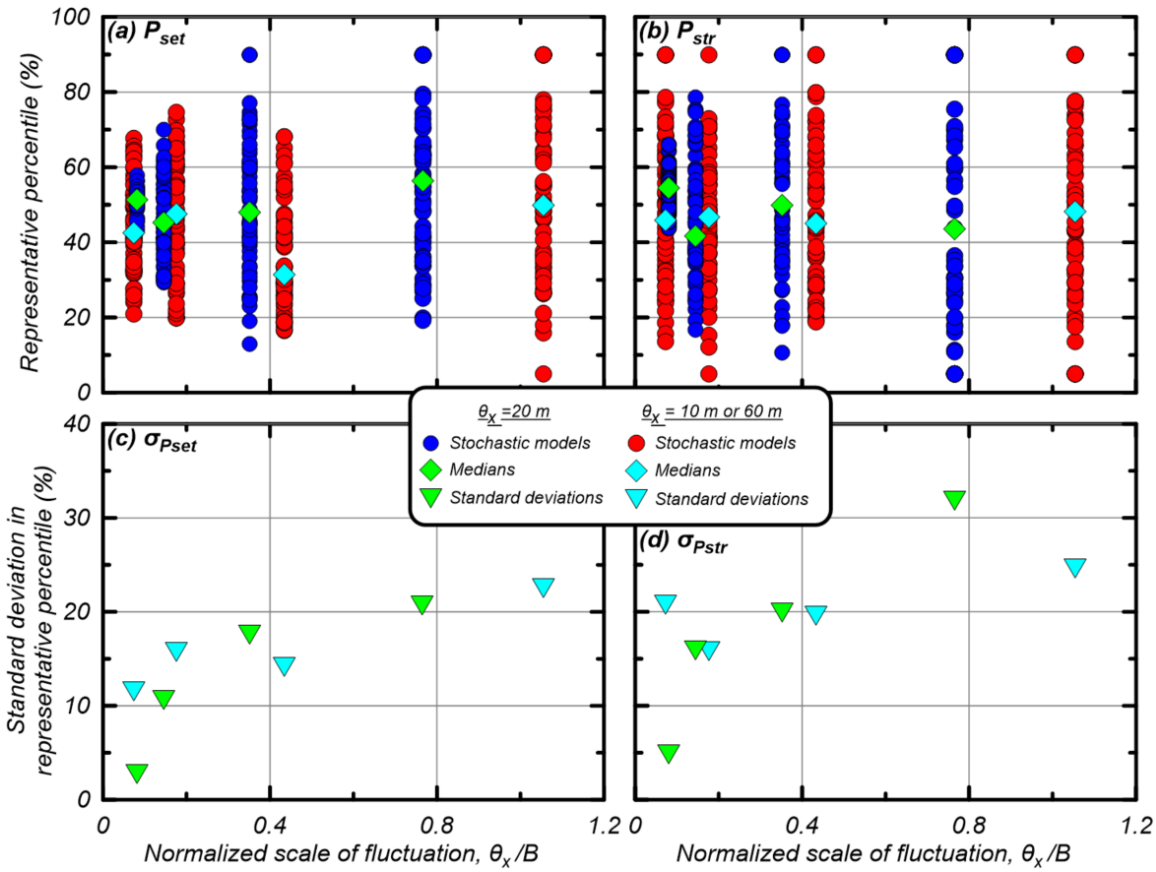

Figure 8: (a) P_{set}, (b) P_{str}, (c) σ_{Pset} and (d) σ_{Pstr} for the original sets of analyses (5, 10, 25 and 45 m high embankments with θ_x = 20 m) with additional analysis sets of the 10 m and 25 m high embankments each with a θ_x = 10 m and 60 m.

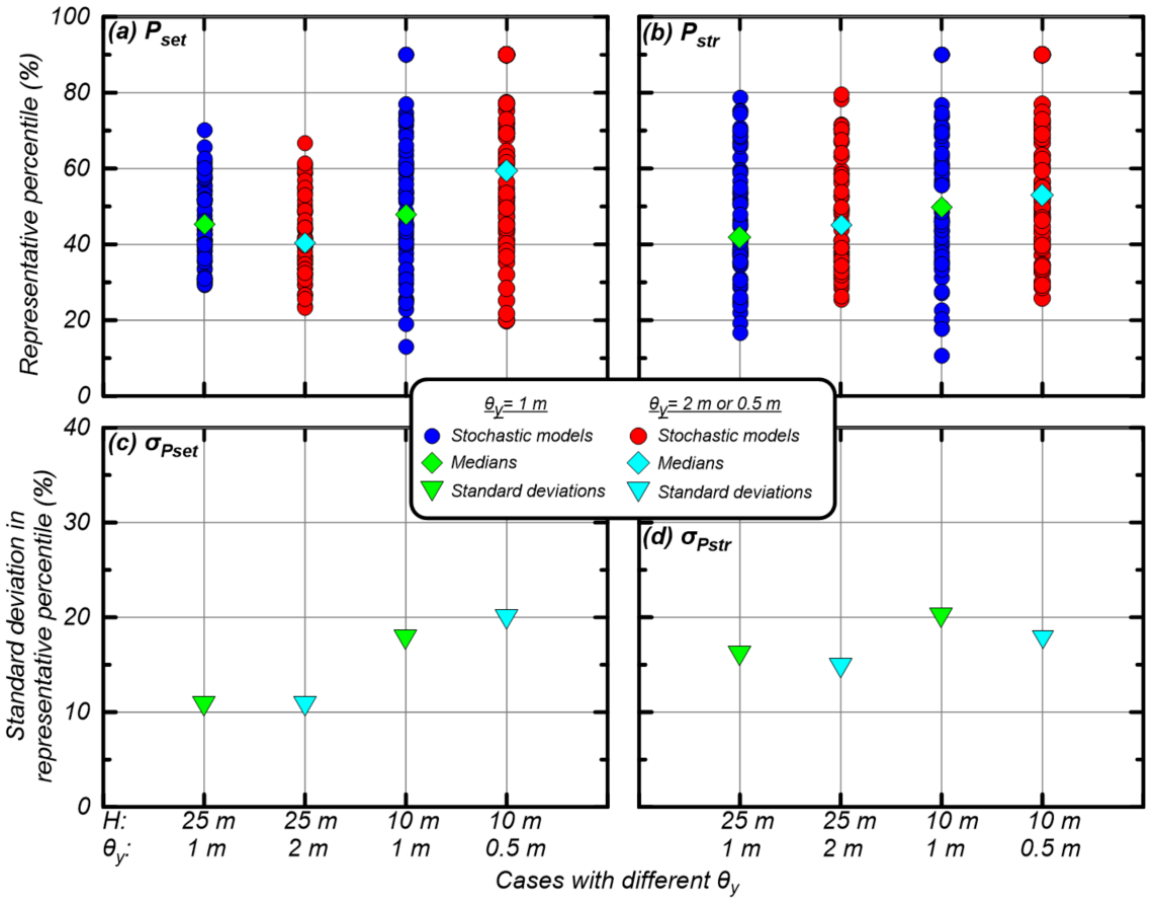

Figure 9: (a) P_{set}, (b) P_{str}, (c) σ_{Pset} and (d) σ_{Pstr} for the 10 m and 25 m tall embankments with θ_x = 20 m and θ_y of 0.5, 1.0, and 2 m subjected to the baseline set of input motions.

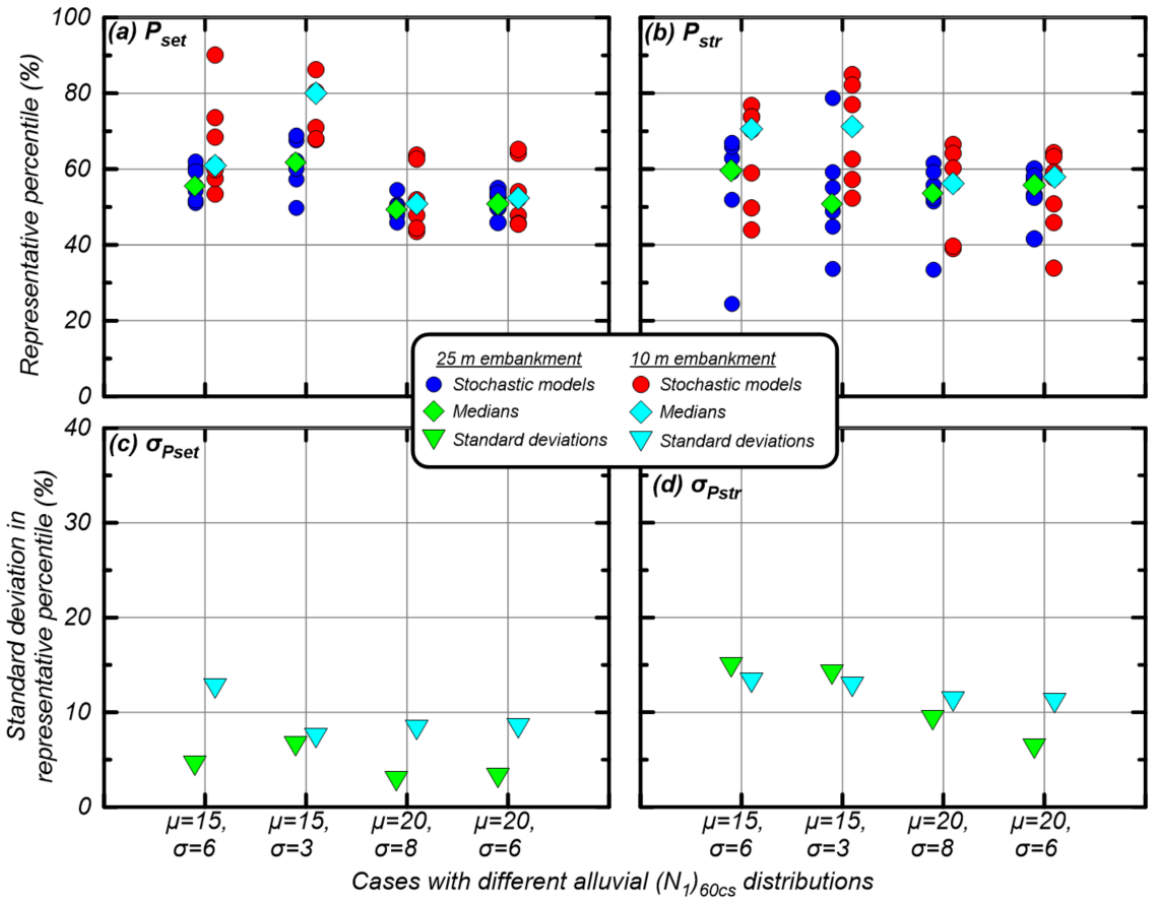

Figure 10: (a) P_{set}, (b) P_{str}, (c) σ_{Pset} and (d) σ_{Pstr} obtained from the 25 m and 10 m embankment dams with θ_x = 20 m and θ_y = 1 m subjected to the TCU motion scaled to a PGA of 0.6 g for the analyses with different means and standard deviations of $(N_1)_{60cs}$.

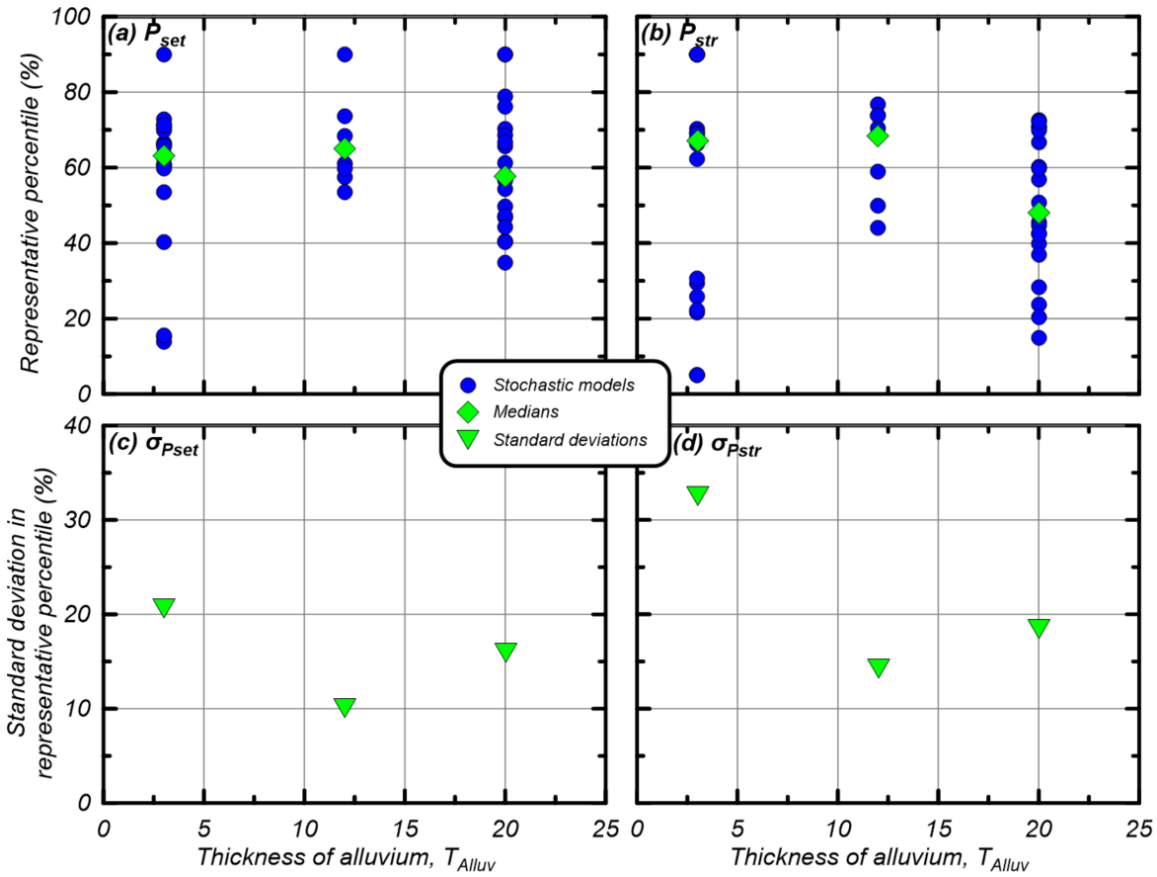

Figure 11: (a) P_{set}, (b) P_{str}, (c) σ_{Pset} and (d) σ_{Pstr} for the 10 m embankment on stochastic alluvium (θ_x = 20 m, θ_y = 1 m) with different thicknesses subjected to the TCU motion scaled to a PGA of 0.6 g.

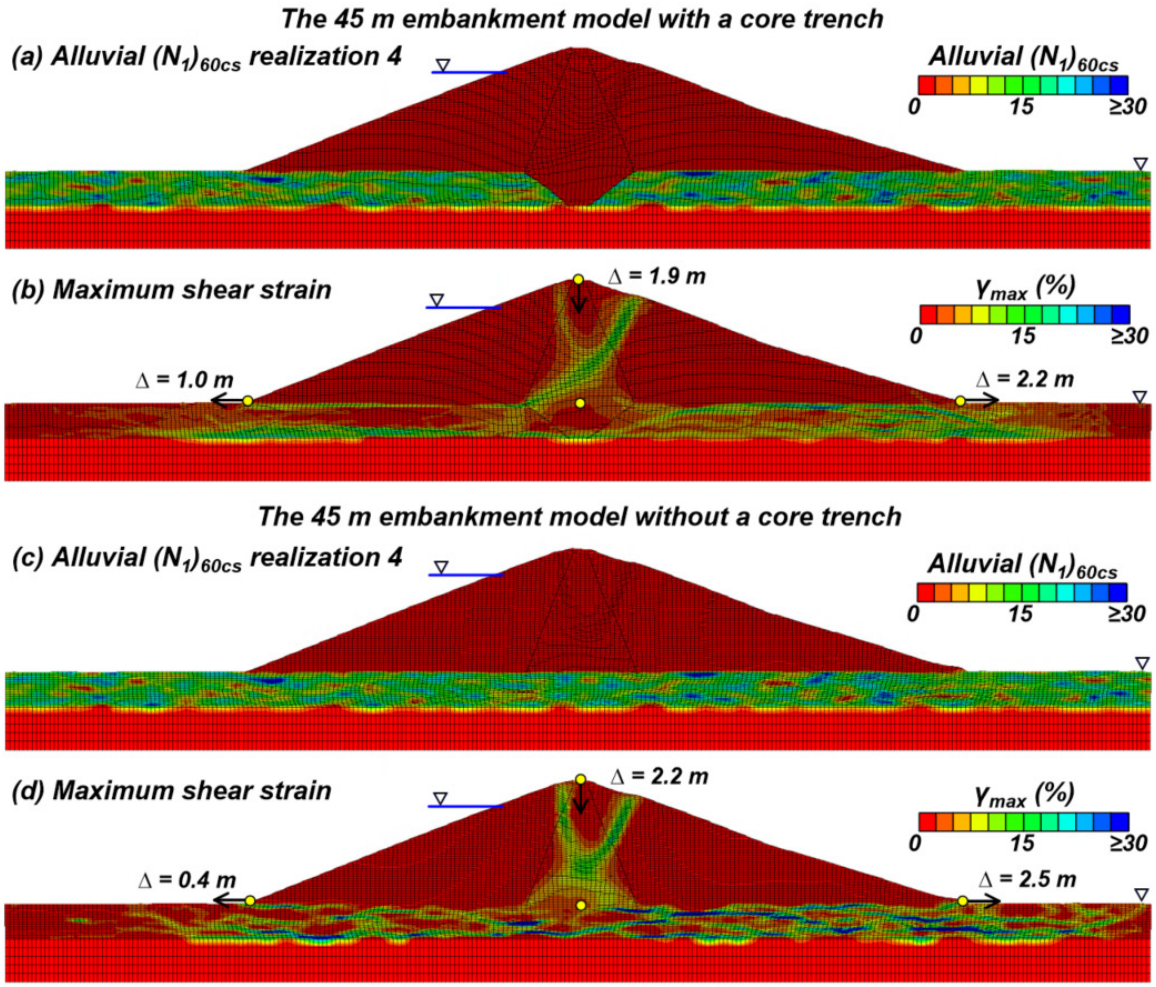

Figure 12: The 45 m embankment model with a core trench subjected to the Mudurnu motion scaled to 0.8 g showing (a) alluvial $(N_1)_{60cs}$ for realization 4, (b) maximum shear strains for a model with alluvial realization 4 and the 45 m embankment model without a core trench subjected to the Mudurnu motion scaled to 0.8 g showing (c) alluvial $(N_1)_{60cs}$ for realization 4, (d) maximum shear strains for a model with alluvial realization 4.

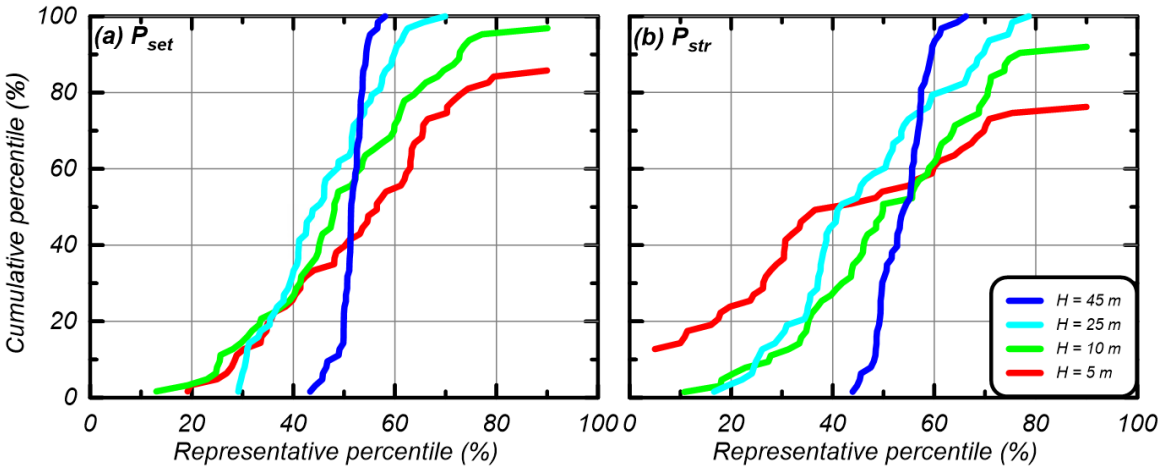

Figure 13: Cumulative percentiles for representative percentiles obtained for the different size embankments in the baseline analyses: (a) P_{set} and (b) P_{str}.

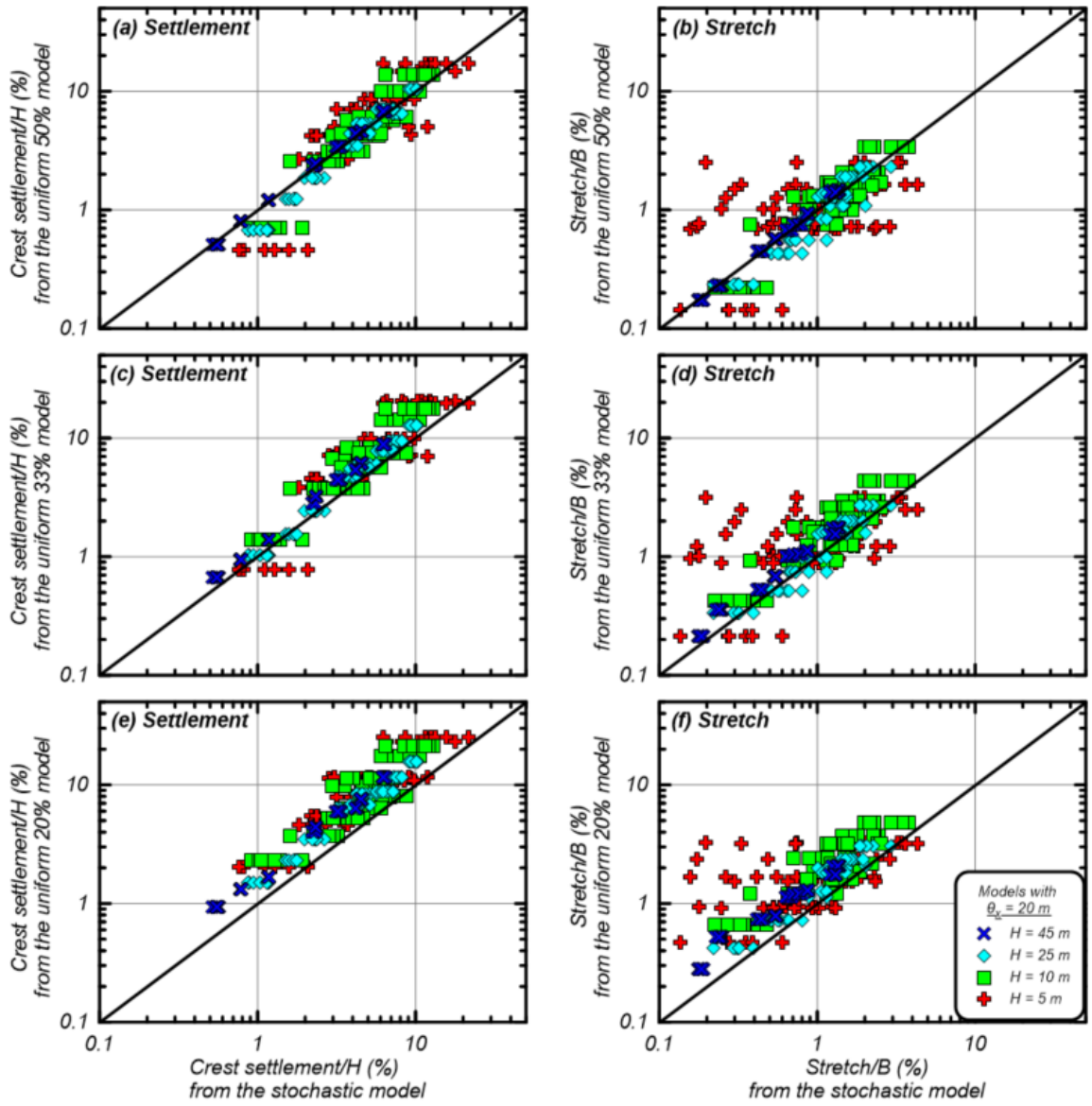

Figure 14: Normalized crest settlements and embankment stretches from the baseline cases of stochastic models versus those obtained using uniform models with: (a, b) 50th percentile $(N_1)_{60cs}$, (c, d) 33rd percentile $(N_1)_{60cs}$, and (d, e) 20th percentile $(N_1)_{60cs}$.

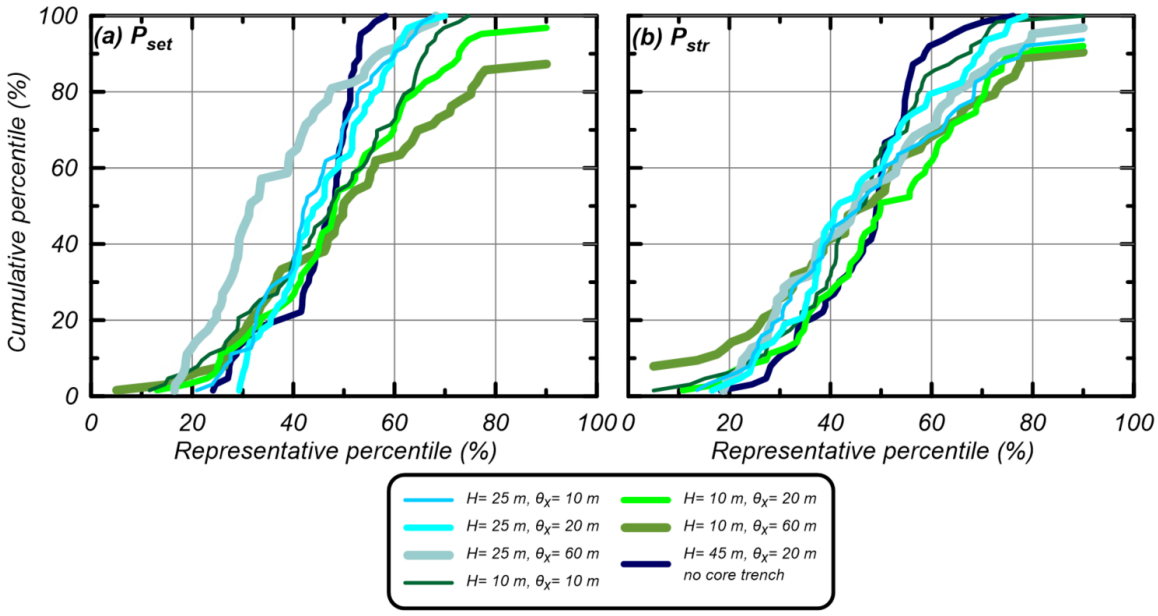

Figure 15: Cumulative percentiles for representative percentiles obtained for the different size embankments with different ratios of θ_x/B: (a) P_{set} and (b) P_{str}.

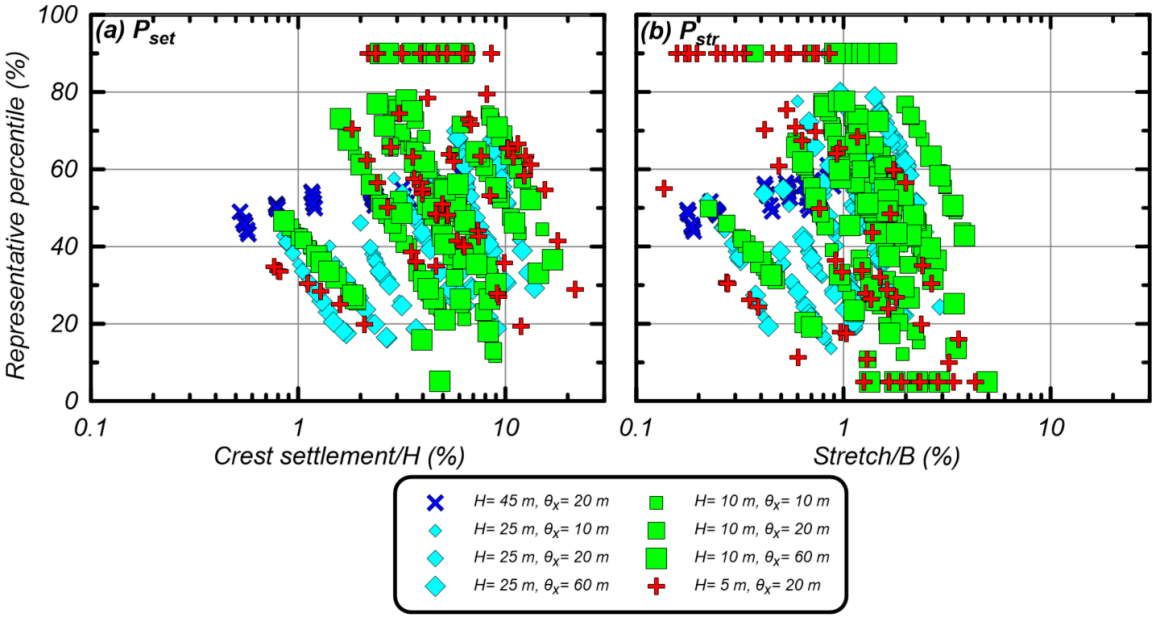

Figure 16: Representative percentiles for normalized deformations obtained for the different size embankments with different ratios of θ_x/B: (a) normalized crest settlement (crest settlement/H) (%) and (b) normalized stretch (stretch/B) (%).